Human Molecular Genetics, 2011, Vol. 20, No. 13 **2524–2534**
doi:10.1093/hmg/ddr151
Advance Access published on April 14, 2011

B9D1 is revealed as a novel Meckel syndrome (MKS) gene by targeted exon-enriched next-generation sequencing and deletion analysis

Katharina Hopp[1], Christina M. Heyer[2], Cynthia J. Hommerding[2], Susan A. Henke[3], Jamie L. Sundsbak[2], Shail Patel[2], Priyanka Patel[2], Mark B. Consugar[2], Peter G. Czarnecki[2], Troy J. Gliem[4], Vicente E. Torres[2], Sandro Rossetti[2] and Peter C. Harris[1,2,*]

[1]Department of Biochemistry and Molecular Biology, [2]Division of Nephrology and Hypertension, [3]Advanced Genomics Technology Center and [4]Department of Laboratory Medicine and Pathology, Mayo Clinic, 200 First Street SW, Rochester, MN 55905, USA

Received December 16, 2010; Revised February 28, 2011; Accepted April 4, 2011

Meckel syndrome (MKS) is an embryonic lethal, autosomal recessive disorder characterized by polycystic kidney disease, central nervous system defects, polydactyly and liver fibrosis. This disorder is thought to be associated with defects in primary cilia; therefore, it is classed as a ciliopathy. To date, six genes have been commonly associated with MKS (*MKS1*, *TMEM67*, *TMEM216*, *CEP290*, *CC2D2A* and *RPGRIP1L*). However, mutation screening of these genes revealed two mutated alleles in only just over half of our MKS cohort (46 families), suggesting an even greater level of genetic heterogeneity. To explore the full genetic complexity of MKS, we performed exon-enriched next-generation sequencing of 31 ciliopathy genes in 12 MKS pedigrees using *RainDance* microdroplet-PCR enrichment and *IlluminaGAIIx* next-generation sequencing. In family M456, we detected a splice-donor site change in a novel MKS gene, *B9D1*. The B9D1 protein is structurally similar to MKS1 and has been shown to be of importance for ciliogenesis in *Caenorhabditis elegans*. Reverse transcriptase–PCR analysis of fetal RNA revealed, hemizygously, a single smaller mRNA product with a frameshifting exclusion of *B9D1* exon 4. ArrayCGH showed that the second mutation was a 1.713 Mb *de novo* deletion completely deleting the *B9D1* allele. Immunofluorescence analysis highlighted a significantly lower level of ciliated patient cells compared to controls, confirming a role for *B9D1* in ciliogenesis. The fetus inherited an additional likely pathogenic novel missense change to a second MKS gene, *CEP290*; p.R2210C, suggesting oligogenic inheritance in this disorder.

INTRODUCTION

In recent years, functional and structural defects in primary cilia have been identified as the cause of an ever-increasing number of inherited diseases with a multi-organ phenotype, the ciliopathies (1,2). Primary cilia are evolutionarily conserved microtubule-based organelles that project from the cell surface and can play an important role in chemo-, mechano- and photosensation (1,2). Their assembly is tightly regulated and originates from the basal body (mother centriole) via protein transport mediated by the intraflagellar transport (IFT) machinery (3). During development, primary cilia have been shown to be crucial for multiple signal transduction pathways (4), including sonic hedgehog that when disrupted can trigger abnormal anterior–posterior patterning of the limb bud, and dorsoventral patterning of the neural tube (5), but also possibly Wnt signaling, including planar cell polarity (6). Due to its multiple roles, disruption of primary cilia results in an array of specific phenotypes that cause a multi-organ disease presentation (see below).

Meckel syndrome (MKS; also called Meckel-Gruber Syndrome [MIM249000,609884]) is a rare (1:10 000–1:140 000),

*To whom correspondence should be addressed. Tel: +1 5072660541; Fax: +1 5072669315; Email: harris.peter@mayo.edu

embryonically lethal, pleiotropic, autosomal recessive disorder, which has been classed as a ciliopathy. Clinical features include bilateral renal cystic dysplasia or polycystic kidney disease (PKD), central nervous system defects (typically occipital encephalocele, but can include the Dandy-Walker malformation or hydrocephalus), postaxial polydactyly and biliary dysgenesis/congenital hepatic fibrosis (7,8). MKS is the most severe ciliopathy, but it has phenotypic and genetic overlap with other viable ciliopathies, such as Joubert syndrome (JBTS [MIM213300]), Bardet–Biedl syndrome (BBS [MIM209900]) and nephronophthisis (NPHP [MIM256100]) (8).

The first two genes associated with MKS were identified in 2006, *MKS1* (17q22 [MIM249000]) and *TMEM67* (*MKS3*; 8q22.1 [MIM609884]; 9,10). Further screening of MKS populations identified: *CEP290* (12q21.3 [MIM610142]), previously associated with NPHP, Senior Loken syndrome [MIM270200], JBTS and Leber congenital amaurosis ([MIM204000]; 11,12); *RPGRIP1L* (16q12.2 [MIM610937]; 13–17), also associated with JBTS with cerebello-renal manifestations; and *CC2D2A* (4q15.33 [MIM612013]; 18), also associated with JBTS (17,19–21). However, mutation screening has suggested that these genes do not account for all MKS families (22). Recently, another MKS gene has been identified, *TMEM216* (11q13.1 [MIM613277]), that also causes JBTS (23,24), while *NPHP3* (*3q22.1* [MIM608002]; 25) and specific BBS genes (*BBS2*, 16q21 and *BBS4*, 15q23 and *MKKS*, 20p12 [MIM606151, 600374, 236700]; 26) have been rarely associated with MKS-like phenotypes (without encephalocele). These further gene identifications illustrate the extreme genetic heterogeneity of MKS, but it seems certain that additional MKS genes are yet to be identified.

Consistent with MKS being a ciliopathy, many of the MKS proteins have been localized to the centrosome, the pericentriolar region, or the cilium itself (1,23,27–29), and loss of the protein is often associated with disrupted ciliogenesis or centrosome defects (18,30–34). Recent advances in genomics allow mutation screening of enriched coding regions of the human genome in combination with next-generation sequencing to identify novel disease genes (35–37). In this study, we employed these methods to screen MKS families for mutations in known ciliopathy genes and others from defined ciliomes. We report the identification of a novel MKS gene, *B9D1*, which is mutated in a pedigree with a severe MKS phenotype, characterized fetal cells from this case and obtained data hinting at oligogenic inheritance.

RESULTS

Mutation screening of the MKS cohort

In our MKS population of 46 families, mutation screening by Sanger sequencing of the most common MKS genes (*MKS1*, *TMEM67*, *TMEM216*, *CEP290*, *CC2D2A* and *RPGRIP1L*; 9,10,12,15,18) revealed two pathogenic variants in only 52% of the pedigrees (38; and manuscript in preparation). The remainder had a single likely pathogenic mutation (9 pedigrees) or no mutation detected (13 pedigrees). To identify novel loci, we enriched and next-generation sequenced the coding exons of 31 genes implicated in ciliopathies or ciliary-related signaling (Table 1) from 12 not fully genetically characterized MKS pedigrees using *RainDance* microdroplet-PCR (39,40) and the *IlluminaGAIIx* with 75 bp paired-end reads. Data were mined using the package Next*GEN*e (SoftGenetics LCC). We employed Sanger-verified single nucleotide polymorphisms (SNPs) detected in the previous screening as positive controls for the optimization of data mining and for the detection of novel variants (see Materials and Methods for details). This analysis identified four novel mutations (see Table 2 and Discussion for details), most interestingly, one in a novel ciliopathy gene, *B9D1*, which has not previously been implicated in MKS or any other ciliopathy.

B9D1 is a novel MKS gene

In pedigree M456, *B9D1* (Chr. 17p11.2; 19.56 kb; 7 exons; CDS 612 bp) had a typical splicing mutation (c.505+2T>C; Fig. 1A–C). This gene was a strong candidate as it is one of three B9 domain-containing proteins, including the MKS protein MKS1, and B9D2 [MIM611951], that appear to have similar cilia-related functions (30,34; see Discussion for details). The typical splicing variant was detected with a sequence depth of 2722 reads and a mutant percentage of 48.79% in the father (R1946) of pedigree M456 (Fig. 1A and B). Sanger sequencing revealed likely hemizygosity of the c.505+2T>C mutation in the fetus since the father was heterozygous for the variant and the mother (R1945) did not carry the mutated allele (Fig. 1C).

RT–PCR amplification of RNA isolated from fetal fibroblasts supported hemizygosity in R1964. The PCR amplification, which spanned all seven exons of *B9D1*, resulted in a single smaller product (416 bp) compared with the normal-sized product of 513 bp (Fig. 1D). This size difference suggested variant-associated exon skipping, which was confirmed by Sanger sequencing. The sequence readout highlighted skipping of exon 4, resulting in a frameshift and a premature stop codon (p.W82CfsX44; Fig. 1E and F) after introduction of 44 non-conserved amino acids and a nearly complete disruption of the functional B9 domain (Supplementary Material, Fig. S1). Evaluation of the mutant protein by exogenous expression of a FLAG-epitope-tagged version of the R1964 transcript further supported the pathogenic nature of the splice mutation. The truncated protein associated with the c.505+2T>C change was not detected when exogenously expressed in U2OS cells, indicative of misfolding and immediate degradation (Supplementary Material, Fig. S2).

ArrayCGH analysis of the fetus and the mother highlighted that the apparent loss of heterozygosity was due to a *de novo* deletion of the *B9D1* locus in the fetus. The deletion spans 1.713 Mb at chromosome 17p11.2, including the complete *B9D1* locus (Fig. 1G). Additionally, 18 other genes were deleted, including the disease locus for the autosomal recessive Sjögren-Larsson syndrome ([MIM 270220]; *ALDH3A2* [MIM609523]), which does not phenotypically overlap with MKS, six snoRNAs and one microRNA of unknown function (Supplementary Material, Table S1).

Table 1. Details of genes screened by exon-enriched next-generation sequencing

Gene[a]	MIM id	Gene id	Chr	Strand	CDS[b] (bp)	Exons[b]	RD amplicon[c]	RD total amplicon length (bp)
B9D2	611951	80776	19q13.2	−	528	4	4	1894
GLIS2	608539	84662	16p13.3	+	1575	6	7	3860
B9D1	N/A	27077	17p11.2	−	932	6	7	3445
ARL6	608845	84100	3q11.2	+	561	9	7	3406
MKKS	604896	8195	20p12	−	1713	4	8	4188
BBS10	610148	79738	12q21.2	−	2172	2	8	4053
INPP5E	613037	56623	9q34.3	−	1935	10	11	5638
ARL13B	608922	200894	3q11.1	+	1287	11	11	5527
BBS5	603650	129880	2q31.1	+	1026	12	11	5578
GLIS3	610192	169792	9p24.2	−	2793	12	12	5854
NEK8	609799	284086	17q11.1	+	2079	14	13	6569
IQCB1	609237	9657	3q21.1	−	1797	15	13	5704
DVL1	601365	1855	1p36	−	2013	15	14	7593
TTC8	608132	123016	14q31.3	+	1548	15	14	7447
MKS1	249000	54903	17q22	−	1680	18	15	6858
BBS1	209901	582	11q13.1	+	1782	17	15	7301
BBS4	600374	585	15q22.3	+	1560	16	16	8449
BBS2	606151	583	16q21	−	2166	17	16	7833
INVS	243305	27130	9q31	+	3198	17	18	9522
NPHP1	607100	4867	2q13	−	2202	20	21	9818
BBS7	607590	55212	4q27	−	2148	19	21	11 175
RPGRIP1L	610937	23322	16q12.2	−	3948	27	25	13 142
IFT88	600595	8100	13q12.1	+	2502	28	26	13 110
TMEM67	609884	91147	8q22.1	+	2988	28	28	13 630
NPHP3	608002	27031	3q22.1	−	3993	27	28	12 862
AHI1[d]	608894	54806	6q23.3	−	3591	30	28	15 046
NPHP4	607215	261734	1p36.22	−	4281	30	29	15 373
TTC21B	612014	79809	2q24.3	−	3950	29	29	14 102
CC2D2A[d]	612013	57545	4p15.32	+	4863	38	35	17 330
CEP290	610142	80184	12q21.32	−	7440	54	50	24 794
PKHD1[d]	606702	5314	6p12.2	−	12 225	68	77	37 682
Total (31 genes)					86 476	618	617	308 783

[a]Genes in boldface are those commonly associated with MKS and those underlined rarely associated with MKS-like phenotypes. *TMEM216* is the sixth gene belonging to this group; however, its association with MKS was discovered after we performed this screen.
[b]The CDS length or exon number is stated as published for the longest isoform of each gene.
[c]Number of *RainDance* (RD) amplicons screened per gene.
[d]These genes have isoforms with additional exons or an exon–intron structure that varies among the isoforms. Additional amplicons were designed for these loci to assure that the CDS of all isoforms was enriched.

Disease presentation in R1964

The affected fetus (R1964) was detected by ultrasound at 13 weeks of gestation with posterior encephalocele and abnormal posterior fossa, bilaterally enlarged multicystic dysplastic kidneys and no bladder. Polydactyly, that is typical in MKS1 (MIM249000) (9), was not noted but the fetus had bilateral club feet and shortened limbs. By 16 weeks, the cystic kidneys were grossly enlarged, distorting the abdomen and compressing the diaphragm. The pregnancy continued until delivery at 35 weeks; the baby survived 1.75 h. Examination at birth indicated an enlarged abdomen, an irregular-shaped posterior encephalocele (2 × 2 × 4 cm), bilateral clubbed feet and ambiguous genitalia. No autopsy was performed. Chromosome analysis of a 400-band karyotype was grossly normal.

B9D1/*B9D2* mutation screening of our MKS cohort

To determine whether B9-containing proteins are more generally associated with MKS, we analyzed 24 not fully genetically resolved MKS pedigrees for *B9D1* and *B9D2* variants. However, we found only common intronic polymorphisms, one synonymous change in *B9D1* (c.594A > C) and two polymorphic missense changes: B9D1, p.R61W and B9D2, p.I11M, all recorded in dbSNP.

R1964 has an additional missense change in *CEP290*

In R1964, we also identified a novel change in a second MKS gene, *CEP290*. Sanger sequencing showed that the heterozygous variant, p.R2210C, was inherited from the mother (Figs. 1A and 2A). The amino acid substitution is located at a well-conserved site in multiple CEP290 orthologs (Fig. 2B) and utilizing various bioinformatics tools the change scored as a highly likely pathogenic change (Table 2), suggesting it is of structural/functional importance. Sanger sequencing and arrayCGH analysis of R1964 did not identify a second *CEP290* mutation. These data highlight possible tri-allelic inheritance that may be playing a role in disease causation or, at least, in modifying the disease presentation.

Analysis of cellular phenotypes in mutant *B9D1* patient fibroblasts

Employing R1964 chorionic villi (CV)-derived fibroblasts, we investigated ciliogenesis compared with karyotypically normal

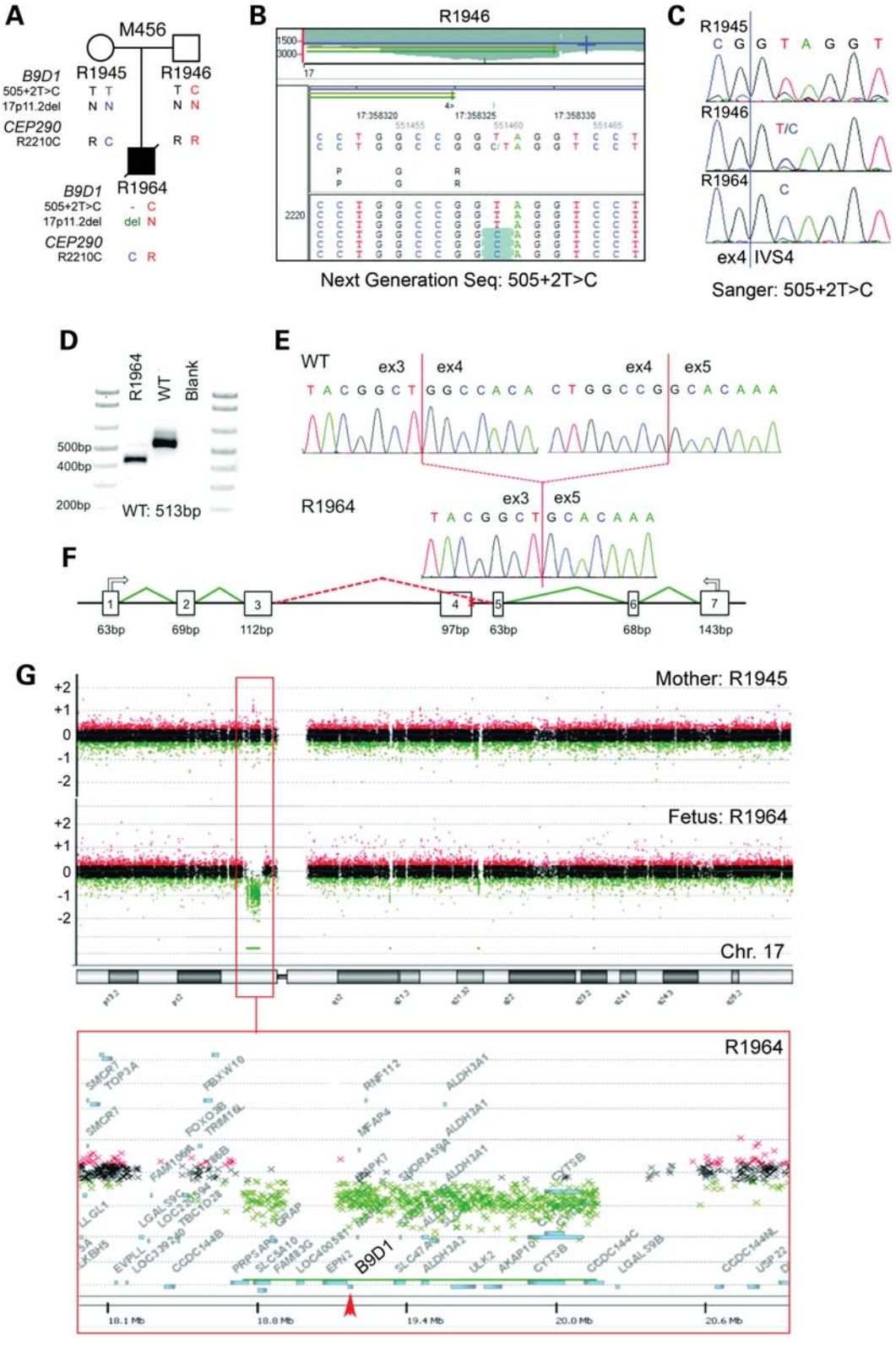

Figure 1. Genetic and functional analysis of the *B9D1* mutations. (**A**) The M456 pedigree shows segregation of the pathogenic *B9D1* mutations and the *CEP290* variant. Alleles inherited paternally are in red, maternal alleles in blue and alleles due to the *de novo* deletion shown in green. The c.505+2T>C *B9D1* splicing change was initially detected by aligning next-generation sequencing reads in Next*GEN*e (**B**) and confirmed in all family members via Sanger sequencing (**C**). RT–PCR analysis of the fetus (R1964) and normal (WT) showed a hemizygous smaller mRNA product (**D**) which excluded *B9D1* exon 4, as demonstrated by sequencing (**E** and **F**). Primer positions are shown (arrows). (**G**) ArrayCGH analysis showed a 1.713 Mb deletion in the fetus, but not in the mother, that removed the *B9D1* gene (arrowhead).

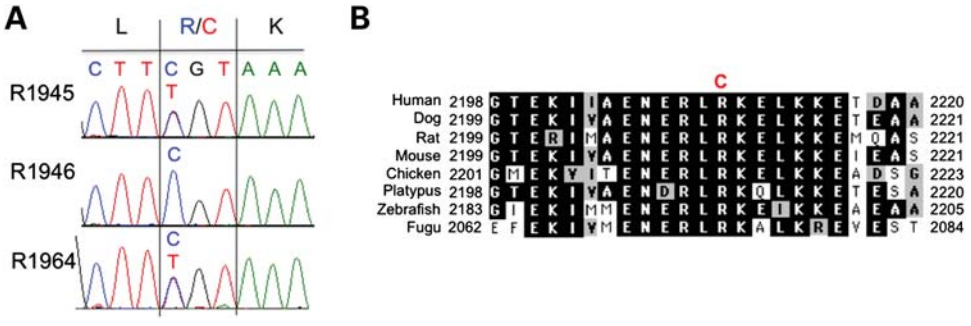

Figure 2. Analysis of the *CEP290* variant p.R2210C. (**A**) Sanger sequencing showing the variant in the mother (R1945) and the fetus (R1964), but not the father (R1946). (**B**) Multi-sequence alignment of CEP290 highlights that this residue is invariant in these species.

CV fibroblasts. Following induction of cilia biogenesis by serum starvation, mutant cells showed a significantly lower level of ciliation (2.9 vs. 45.3% $P < 0.0001$) compared with the normal cells (Fig. 3A–C). In addition, in the small number of R1964 cells that formed primary cilia, it appears that cilia biogenesis may be impaired as the cilia appeared shorter and not as well defined as in the control cells (Fig. 3B, bottom panel). Centrosome duplication defects, which have previously been associated with *MKS1* mutations (31), were also observed in the R1964 cells at a higher percentage (24.3 vs. 8.5% $P = 0.0025$) compared with the normal cells (Fig. 3C).

CEP290 localization

Given the additional *CEP290* mutation (p.R2210C) found in this family, we analyzed the localization of this protein in the R1964 fibroblasts. Previously, CEP290 was found to co-localize with the centriolar satellite protein PCM-1, scattered around the centrosome, while CEP290 depletion was shown to disrupt PCM-1 protein complex formation (41). Consistent with these data, we observed aggregation of CEP290 around the centrosomes and centrioles in three representative patterns of variable diffusion (Fig. 3D). However, there were no notable localization differences observed between the mutant R1964 cells and a human placental fibroblast cell line. Depending on the stability of the mutant protein, this localization may represent protein derived from both alleles or from just the normal protein.

DISCUSSION

We used a combination of two novel technologies (PCR-based exon-enrichment and next-generation sequencing) to explore the genetic complexity of 12 genetically unresolved MKS pedigrees. This led to the identification of four novel variants including the typical splicing change (c.505 + 2T > C) in a novel MKS/ciliopathy gene, *B9D1* (Fig. 1 and Supplementary Material, Fig. S1), and subsequent analyses revealed a *de novo* deletion of the normal allele. Further, we highlighted potential oligogenic inheritance or modifying effects in the pedigree since the fetus inherited a single likely pathogenic missense change in a second MKS gene, *CEP290* (Fig. 2).

B9D1 is evolutionarily conserved in ciliated organisms and localizes to the basal body and primary cilia in mammalian cells, and to the transition zone in *Caenorhabditis elegans* (30,34). The protein has also been shown to interact with the other B9 domain proteins, B9D2 and MKS1 by yeast two-hybrid analyses (42), while in *C. elegans* these proteins are thought to complex at the base of the cilium (34). Additionally, depletion of *B9D1* by shRNA has been shown to decrease cilia number in mIMCD3 cells (30). Consistent with this, the M456 fetal cells (that have likely completely lost functional B9D1; Supplementary Material, Figs. S1 and S2) had a very low level of ciliated cells compared with the control.

B9-containing proteins are also implicated in cilia biogenesis/function in whole organisms where knockdown or conditional deletion of *B9D2* results in defects in cilia stability/formation in *Paramecium tetrauelia* (43) and in impaired ciliogenesis, cystic kidney disease and hydrocephalus in the *stumpy* mouse mutant (44). The phenotype observed in R1964 is similar to *stumpy* or to MKS1 (9,33), with the notable exception of bilateral club feet rather than the polydactyly typically seen in MKS1. It seems unlikely that such a severe reduction in ciliated cells as observed in the R1964 mutant fibroblasts can occur in every tissue as this would be unlikely compatible with the degree of fetal development seen here. For example, a knockout mouse model of the IFT protein IFT88 [MIM600595] (45) displays early to mild-gestation lethality due to complete loss of cilia biogenesis. Instead, it is likely that tissue-specific reductions in ciliation occurred in the fetus, as has been reported in ciliopathy knockout mouse models of *MKS1* and *RPGRIP1L* (28,46).

Oligogenic inheritance has been suggested in BBS, a milder ciliopathy. There, both triallelism and digenic inheritance (47), as well as alleles from a second gene significantly modifying the phenotype (48), have been reported. Recently, single possible mutant alleles of two genes, *WDPCP* [MIM613580] and *TTC21B* [MIM612014], implicated in other ciliopathies, have also been described in MKS patients (49,50). In two other patients in our screen, single strongly scoring variants in *NPHP3* or the autosomal recessive PKD (ARPKD [MIM2632001]) gene, *PKHD1* [MIM606702] (this variant was previously described as an ARPKD mutation; 51) were detected in combination with one or two *CC2D2A* mutations (Table 2), further emphasizing genetic complexity in MKS.

Table 2. Summary of novel variants detected by the *RainDance* screen

Pedigree	Origin[a]	Mutations						Other Variant					
		Gene	Designation[b]	Evaluation[c] Align GVGD	SIFT	PolyPhen	Con	Gene	Designation[b]	Evaluation[c] Align GVGD	SIFT	PolyPhen	Con
M456	M							*CEP290*	p.R2210C	C65 (B)	0 (B)	2.23 (B)	B
	P	*B9D1*	**c.505 + 2T > C**				A		NOVD				
	F		Del1.7Mb				A						
M454	M	*CC2D2A*	c.2778del5				A	*NPHP3*	**p.N386S**	C45 (C)	0 (B)	1.41 (C)	C
	P		NMD						NOVD				
M459	M	*TMEM67*	p.R549C	C65 (B)	0 (B)	2.49 (B)	B						
	P		**p.G250R**	C65 (B)	0 (B)	2.17 (B)	B						
M506[d]	M	*CC2D2A*	c.3084delG				A	*PKHD1*	**p.C3346R**	C65 (B)	0 (B)	3.17 (B)	B
	P		c.3084delG				A		NOVD				

Variants detected by the *RainDance* screen are bolded.
[a]Parental origin of mutation; M, maternal; P, paternal, F, *de novo* change only found in fetus. All parental changes segregated to the fetus.
[b]NMD, no mutation detected; NOVD, no other variant detected.
[c]Con, consensus mutation score from all evaluation tools. A, definite truncating mutation; B, highly likely mutation; C, likely mutation.
[d]The *CC2D2A* mutations were detected by Sanger sequencing after the *RainDance* screen began and confirmed by the *RainDance* analysis.

The significance of the *CEP290* mutant allele in addition to the loss of B9D1 in M456 is unclear. The importance of *CEP290* as a MKS disease gene is well documented (11,12)—in our population 13% (6/46) of pedigrees have two *CEP290* mutations, making it one of the most frequent MKS genes (manuscript in preparation). Its role as a key player in oligogenic inheritance or as a modifier is further supported in our population in which three additional families had one likely *CEP290* mutation—one with a single pathogenic mutation, one with a *CEP290* nonsense mutation and a strongly scoring *RPGRIP1L* missense variant and the third with two strongly scoring missense changes to *CEP290* and *CC2D2A* (manuscript in preparation).

In the M456 family, the additional *CEP290* mutation could possibly be associated with the severe limb phenotype. Also, the *CEP290* variant may explain why *B9D1* is only rarely a cause of MKS. The combination of an additional variant in a *B9D1* mutation background as reported here is especially interesting since additional loss of the NPHP genes *nphp-1* (MIM607100) or *nphp-4* (MIM606966) is required to disrupt ciliation in *C. elegans* B9 protein mutants (30,34). On the other hand, recessive mutations at *MKS1* alone generate a severe MKS phenotype (9), and conditional loss of *B9D2* in the mouse generates an MKS-like phenotype (44). Also, *B9D1* is a small gene (small mutational target) and *MKS1* is only a common cause of MKS because of the Finnish ancestral mutation (9).

Recently, next-generation sequencing was employed to identify mutations in conventionally PCR-amplified exons of 18 NPHP ciliopathy genes, identifying mutations in 30/120 NPHP families (52). Here we have extended this approach to employ exon-enrichment and next-generation sequencing to identify a novel MKS gene and reveal genetic complexity using micro-droplet PCR amplified exons. The high level of sensitivity (see Materials and Methods) that we obtain in our experiment is illustrated by the identification of a *TMEM67* variant (G250R; M459) that was previously missed by Sanger sequencing in a patient with a second *TMEM67* change (Table 2). Since this technology has the potential to be scaled to screen ∼2300 genes (39,40) in a single reaction, exceeding the number of genes currently annotated in the human ciliome (∼2024 genes) (53); we believe this may be a suitable method for screening a large, defined number of candidates that are justified biologically. Consequently, this approach should be considered a viable option compared with whole-exome analysis for mutation screening ciliopathy pedigrees while allowing pooling of indexed samples to reduce sequencing costs.

In conclusion, we provide strong evidence that *B9D1* is a novel MKS gene. The initial mutation was identified using the novel approach of *RainDance* exon-enrichment and next-generation sequencing, highlighting its suitability to characterize complex human diseases, such as ciliopathies. That we detected *B9D1* mutations in only one pedigree emphasizes the genetic heterogeneity of MKS. The cellular phenotype we observed in mutant fibroblasts highlighted the importance of B9D1/CEP290 in ciliation, and stresses the fact that *B9D1* should be considered in MKS and other ciliopathy diagnostic testing. Additionally, our data emphasize that *CEP290* alleles may act as disease modifiers in MKS.

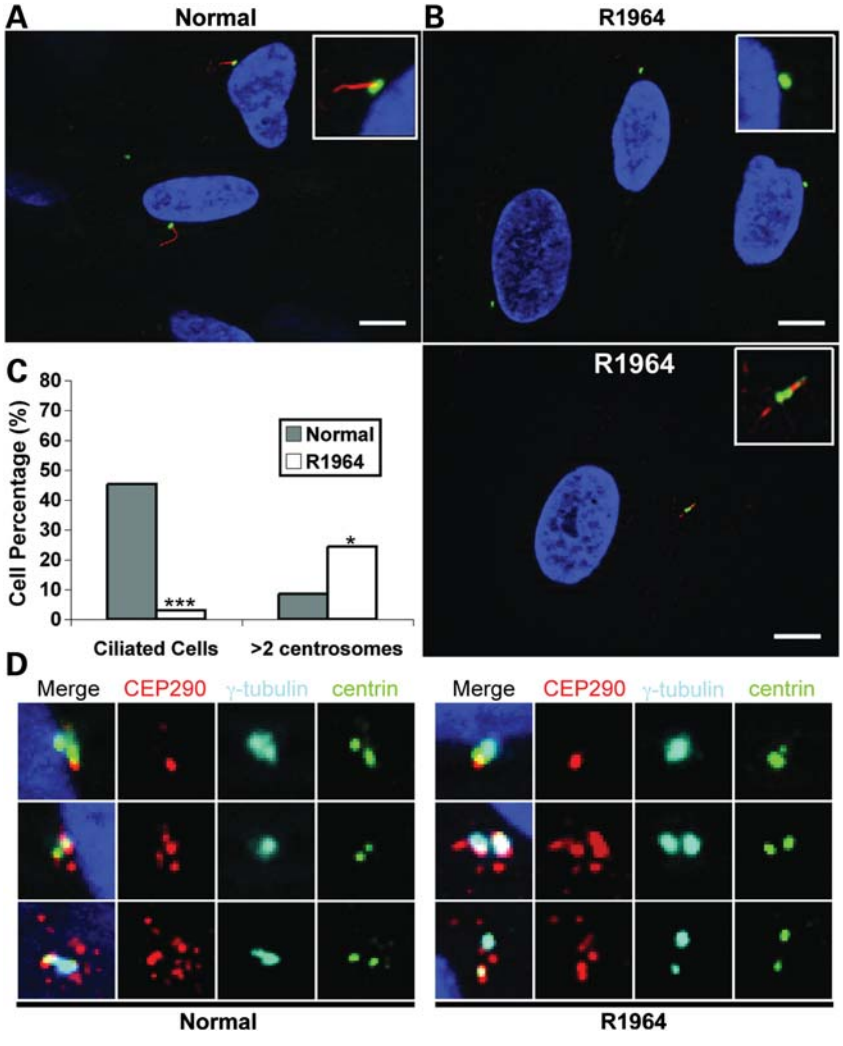

Figure 3. Cilia morphology analysis of R1964 by immunofluorescence microscopy. Analysis of ciliogenesis showed many fewer ciliated cells in the R1964 CV cells (**B**) in comparison to the control CV cells (**A**), with the occasionally ciliated R1964 cells having very short cilia (B; bottom panel). Cilia were stained with acetylated α-tubulin (red) and centrosomes were stained with γ-tubulin (green); scale bar equals 10 μm. (**C**) Quantification of ciliated cells and abnormal number of centrosomes in R1964 and normal controls highlights ciliation of fewer mutant fibroblasts; $^{***}P < 0.0001$ and a greater percentage of cells with an abnormal number of centrosomes; $^{*}P = 0.0025$. At least one hundred cells were counted and statistically analyzed using a two-tailed Fisher's exact test. (**D**) CEP290 centriolar satellite localization is not clearly different between R1964 and a control placental fibroblast cell line.

MATERIALS AND METHODS

Patient population and recruitment

This study was approved by the relevant Institutional Review Boards, and all family members gave informed consent. Family M456 was a non-consanguineous family referred for research testing from within the USA. All clinical records were reviewed by an experienced clinician. Blood samples were collected from parents, and CV cells and fetal tissue were available from the fetus, for DNA extraction and phenotypic analysis. DNA was isolated utilizing the Qiagen *Puregene* kit.

Sanger mutation screening

Initial mutation screening was performed by conventional Sanger sequencing after PCR amplification of all coding exons (± 20 bp). PCR amplification was performed using the *PlatinumTaq* protocol (Invitrogen) with an annealing temperature range of 58–62°C and an elongation time of 1 min/kb. M13-tailed sequencing primers were used for amplification allowing a standardized sequencing reaction that was outsourced to *Beckman Coulter Genomics*.

Gene selection and primer design for *RainDance* enrichment

The 31 genes (Table 1) were selected from the Cilia Proteome v3.0 Database (http://v3.ciliaproteome.org/cgi-bin/index.php) and prioritized for screening based on their direct implication as a ciliopathy gene or *in vivo* data supporting their cilia-dependent signaling role. The primer design was performed by *RainDance* using the *Primer3* software. The primers had a standard annealing temperature of 57–59°C amplifying a

product between 250 and 600 bp. We excluded all amplicons that amplified non-coding exons. *RainDance* synthesized the primers and performed droplet PCR exon enrichment utilizing the RDT-1000.

Amplicon concatenation

After exon enrichment, the samples had a concentration between 30 and 72 ng/μl with a total volume of 10 μl. Successful enrichment was tested by *RainDance* utilizing the Agilent Bioanalyzer *DNA 12000* kit. All samples had the greatest size frequency between 300 and 700 bp. Prior to sequencing, the samples were blunt-ended and 5′ phosphorylated using the *Quick Blunting Kit* (New England Biolabs; NEB) and concatenated with the *T4 Quick Ligase Kit* (NEB) to enable successful random fragmentation during the next-generation sequencing library preparation. For optimal ligation, 5 μl of T4 ligase was added three times, first after 4 h then twice after 8 h. The ligase was inactivated by adding ethylenediaminetetraacetic acid (EDTA) (30 mM). Successful concatenation was tested using the Agilent Bioanalyzer *DNA High Sensitivity* kit. The maximum fragment size of each sample ranged between 2500 and 10 000 bp, while only a minute fraction (less than 10%) remained unconcatenated.

Next-generation sequencing

Sample library preparation and next-generation sequencing were performed at the Mayo Clinic Advanced Genomics Technology Center. The concatenated samples were sonicated using the *Covaris E210* (duty cycle: 10%, intensity: 5, and burst: 200) and library preparation was performed using the *Illumina Next Reagents* (NEB). Successful library preparation was checked using the Agilent Bioanalyzer *DNA 7500* and sequenced on the *IlluminaGAIIx* using 75 bp paired-end indexed reads. Initial cluster formation was performed on 7 pM of enriched/concatenated/sonicated DNA using the *Illumina Cluster Station*. A final cluster density with an average of 217 594 clusters/lane was sequenced, followed by individual read base calling using the *Pipeline* v2.0 software (Illumina).

Next-generation data analysis

The next-generation sequencing reads were analyzed using the variant discovery software Next*GEN*e (SoftGenetics LLC). The reads were aligned against the GenBank file of the 31 genes and their isoforms. For reliable Indel discovery, we utilized one cycle of consolidation when analyzing the data. Consolidation aligns the paired-end reads, merges overlapping sequences and creates a consensus sequence by elongating the original read while maintaining the information of that read. Consequently, reads with larger Indels are less likely disregarded as poorly resolved sequence. For a variant to be called, we required the read containing the variant to match 80% to the aligned position, the variant to be covered by at least 30 reads and the variant to be present in 10% of all reads aligned to the given position. To filter all detected variants meeting the given criteria, we used Sanger-detected SNPs of each pedigree as a baseline. First, we assured 100% sensitivity of all prior Sanger-sequenced SNPs using these criteria. Next, we determined the SNP with the lowest coverage of reads and the SNP with the lowest mutant percentage. Both parameters were then used to detect novel variants by filtering the initial report for variants that had at least one-half of the lowest coverage and one-half of the lowest mutant percentage of any known SNP. Overall, we obtained a specificity of 99.19% covering 613/618 exons with a mean coverage greater than 100-fold. Multiplexing of three indexes in one lane (one index/sample) obtained on average 24 105 total reads of which 76.49 ± 1.82% mapped to the target region. All positive controls had a mean coverage of 3224 ± 2827 fold if multiplexing three indexed samples per lane.

Variant analysis

All identified novel variants were analyzed for their potential pathogenic character utilizing various bioinformatics tools. First, they were compared against the dbSNP 131 database. Variants recorded as known SNPs were excluded from further analysis and scored as likely polymorphic. Subsequently, all remaining missense changes were scored for likely pathogenicity utilizing *AlignGVGD* (http://agvgd.iarc.fr/agvgd_input.php), *SIFT* (http://sift.jcvi.org/) and *PolyPhen* (http://genetics.bwh.harvard.edu/pph/index.html). Multi-sequence alignments contained at least eight orthologs, including mammals, birds and fish for the *AlignGVGD* and *SIFT* analysis. Variants were designated as highly likely (B) or likely (C) pathogenic as previously described (54). Variants that scored as likely pathogenic with two of the bioinformatics tools were checked for segregation within the family employing Sanger sequencing. Segregation as well as bioinformatics analysis of novel variants is summarized in Table 2.

Variant confirmation

The segregation of the two detected variants in M456, *CEP290:* p.R2210C and *B9D1:* c.505 + 2T > C, was analyzed by Sanger sequencing. To re-sequence the Next*GEN*e-detected variants, the exon containing the change was PCR amplified using primers located in the flanking introns.

CEP290	Forw-IVS46	5′-ACGTTGGGAACTTCGTTCTCAC-3′
	Rev-IVS47	5′-GGCATAGAAACACAATTCCTCAATC-3′
B9D1	Forw-IVS3	5′-GCTCCATCCTTTGAGCACCC-3′
	Rev-IVS4	5′-GAGCATTCCCAGCCTGAACC-3′

The PCR products were purified (*ExoSAP-IT*, Affymetrix) and sequenced on the *ABI PRISM 3730xl* DNA analyzer. Sequence analysis was performed with the *Sequencher* v4.8 software (Gene Code Cooperation). Similar segregation analysis was done for other detected variants (Table 2).

ArrayCGH

The arrayCGH analysis was performed at the Mayo Clinic Cytogenetics Laboratory. We provided 1 μg of fetal DNA (isolated from fetal tissue) and blood DNA from the mother to run the array. In order to cover the region surrounding *B9D1* on chromosome 17 and *CEP290* in high density, we ran a one million-feature chip on both samples (Agilent

SurePrint G3 1X1M). We analyzed the array data using the *Genomic Workbench* v5.0 software (Agilent).

cDNA analysis

RNA was isolated from the fetal-derived cell line and from a normal 20-week gestation placental cell line (CRL-7548-ATCC) using the *RNAeasy* kit (Qiagen). cDNA was synthesized by RT–PCR utilizing the *Superscript III* kit (Invitrogen). To assess whether the *B9D1* variant altered splicing, we PCR amplified the cDNA using a forward and reverse primer within the first and last coding exon of the gene.

B9D1 c.505 + 2T > C	Forw-ex1	5′-TTCTACTCATGGTCAA CGGGCAGG-3′
	Rev-ex7	5′-TTCCTCATGTCCTTGG TCACCACG-3′

The amplicons of the normal and the fetal (R1964) cDNA were assessed by agarose gel electrophoresis (1.5% agarose gel) and by Sanger sequencing.

Cloning of the N-terminally tagged *B9D1* WT and R1964 mutant constructs

Full-length WT *B9D1* was amplified from a HEK293T cDNA preparation using a forward primer linked to a *Bam*H I site followed by the start codon of *B9D1* and a reverse primer linked to a *Not*I site after the stop codon of *B9D1* (restriction sites: *italics*, Start/Stop codon: bold).

Forw-BamHI	5′-CGC*GGATCC***ATG**GCGACCGCGAGTCCTAGC-3′
Rev-NotI	5′-TTTTCCTTTT*GCGGCCG**C**T**A**C*TGGGGGAAGCT CTGGGG-3′

The WT *B9D1* amplicon was cloned into pcDNA3.1(+) FLAG-*Bam*H I. The c.505 + 2T > C mutant allele (with a frameshifting deletion of exon 4) was cloned from a cDNA preparation of R1964 primary CV cells (see cDNA analysis above). Using unique internal restriction sites (*Nco*I—start codon; *Dra*III—exon 7), the mutant cDNA was cloned into the 3X-FLAG-WT *B9D1* pcDNA3.1(+) construct.

Expression analysis of the *B9D1* constructs

The N-terminal FLAG-tagged cDNA constructs were transfected into U2OS cells using electroporation (Nucleofector II, Amaxa). The cells were selected using 300 μg/ml of geneticin (G418, Invitrogen) for 72 h. Whole cell lysates were isolated using RIPA buffer (Upstate) and total RNA extractions performed as described above. Protein expression analysis was performed by western blotting with 20 μg of protein loaded on a 4–12% Bis–Tris gel (Invitrogen) and transferred onto a 0.4 μm polyvinylidene fluoride membrane. The exogenous B9D1 product was detected using the α-FLAG antibody (F7425; Sigma) and the α–γ-tubulin antibody (T6557; Sigma) was used as a loading control.

Fibroblast cell culture and ciliogenesis induction

Cells from fetus R1964 were collected by chorionic villus sampling (CVS) and compared with normal primary CV fibroblasts (obtained from a phenotypically and karyotypically normal fetus). Fibroblasts were cultured in advanced DMEM/F-12 (Invitrogen) supplemented with 30% fetal bovine serum (FBS), glutamine, penicillin/streptomycin (Gibco) and plasmocin (InvivoGen). Prior to analysis, cells were grown to confluence, and serum starved (0% FBS) to induce ciliation and grown for an additional 3 days. In cells prepared for CEP290 analyses, ciliation was not induced and a normal placental fibroblast cell line (ATCC, CRL-7548) was employed as a control (cultured in same media supplemented with 5% FBS).

Immunofluorescence microscopy

Antibodies. Monoclonal antibodies T6793 and T6667 (Sigma) to acetylated α-tubulin and γ-tubulin were employed to label cilia and centrosomes, respectively. For CEP290 localization studies, a polyclonal antibody against CEP290 (NB100-86991; Novus Biologicals; recognizing residues 2429–2479) and a monoclonal antibody against centrin (20H5, Dr Jeffrey Salisbury, Mayo Clinic, Rochester) were also employed.

Immunolabeling. All cells were fixed in methanol and prepared for analyses as described previously (31). Slides were visualized using a Zeiss AxioObserver (Carl Zeiss) microscope at a magnification of ×100.

Statistical analysis

Statistical significance of cell phenotypes were determined as previously described (31).

SUPPLEMENTARY MATERIAL

Supplementary Material is available at *HMG* online.

ACKNOWLEDGEMENTS

We wish to thank Drs Eric Wieben and Franklyn Prendergast (Mayo Center of Individualized Medicine) for support and encouragement; Bruce Eckloff and Yean Kit Lee for technical assistance; Vickie Kubly for coordinating sample collection; Dr Daniel Van Dyke for making available the normal CVS cells; and Dr Jeffrey Salisbury for kindly providing the centrin antibody. MKS families and referring physicians and counselors are thanked for their participation.

Conflict of Interest statement. None declared.

FUNDING

This work was supported by a grant from the Bernard E. and Edith B. Waterman Charitable Foundation through the Center of Individualized Medicine, Mayo Clinic; the National

Institute of Diabetes and Digestive and Kidney diseases (grant number DK059597); and Mayo Graduate School (K.H.).

REFERENCES

1. Fliegauf, M., Benzing, T. and Omran, H. (2007) When cilia go bad: cilia defects and ciliopathies. *Nat. Rev. Mol. Cell Biol.*, **8**, 880–893.
2. Tobin, J.L. and Beales, P.L. (2009) The nonmotile ciliopathies. *Genet. Med.*, **11**, 386–402.
3. Pedersen, L.B., Veland, I.R., Schroder, J.M. and Christensen, S.T. (2008) Assembly of primary cilia. *Dev. Dyn.*, **237**, 1993–2006.
4. Goetz, S.C. and Anderson, K.V. (2010) The primary cilium: a signalling centre during vertebrate development. *Nat. Rev. Genet.*, **11**, 331–344.
5. Wong, S.Y. and Reiter, J.F. (2008) The primary cilium at the crossroads of mammalian hedgehog signaling. *Curr. Top Dev. Biol.*, **85**, 225–260.
6. Wang, B., Sinha, T., Jiao, K., Serra, R. and Wang, J. (2010) Disruption of PCP signaling causes limb morphogenesis and skeletal defects and may underlie Robinow syndrome and brachydactyly type B. *Hum. Mol. Genet.* [epub ahead of print]. doi:10.1093/hmg/ddq1462.
7. Ahdab-Barmada, M. and Claassen, D. (1990) A distinctive triad of malformations of the central nervous system in the Meckel-Gruber syndrome. *J. Neuropathol. Exp. Neurol.*, **49**, 610–620.
8. Harris, P.C. and Torres, V.E. (2009) Polycystic kidney disease. *Annu. Rev. Med.*, **60**, 321–337.
9. Kyttala, M., Tallila, J., Salonen, R., Kopra, O., Kohlschmidt, N., Paavola-Sakki, P., Peltonen, L. and Kestila, M. (2006) *MKS1*, encoding a component of the flagellar apparatus basal body proteome, is mutated in Meckel syndrome. *Nat. Genet.*, **38**, 155–157.
10. Smith, U.M., Consugar, M., Tee, L.J., McKee, B.M., Maina, E.N., Whelan, S., Morgan, N.V., Goranson, E., Gissen, P., Lilliquist, S. *et al.* (2006) The transmembrane protein meckelin (*MKS3*) is mutated in Meckel-Gruber syndrome and the wpk rat. *Nat. Genet.*, **38**, 191–196.
11. Frank, V., den Hollander, A.I., Bruchle, N.O., Zonneveld, M.N., Nurnberg, G., Becker, C., Bois, G.D., Kendziorra, H., Roosing, S., Senderek, J. *et al.* (2008) Mutations of the *CEP290* gene encoding a centrosomal protein cause Meckel-Gruber syndrome. *Hum. Mutat.*, **29**, 45–52.
12. Baala, L., Audollent, S., Martinovic, J., Ozilou, C., Babron, M.C., Sivanandamoorthy, S., Saunier, S., Salomon, R., Gonzales, M., Rattenberry, E. *et al.* (2007) Pleiotropic effects of *CEP290* (*NPHP6*) mutations extend to Meckel syndrome. *Am. J. Hum. Genet.*, **81**, 170–179.
13. Wolf, M.T.F., Saunier, S., O'Toole, J.F., Wanner, N., Attanasio, M., Salomon, R., Groshong, T., Sayer, J.A., Oh, J., Neuhaus, T.J. *et al.* (2007) Mutational analysis of *RPGRIP1L* gene in 56 patients with Joubert syndrome and nephronophthisis. *Kidney Int.*, **12**, 1520–1526.
14. Arts, H.H., Doherty, D., van Beersum, S.E., Parisi, M.A., Letteboer, S.J., Gorden, N.T., Peters, T.A., Marker, T., Voesenek, K., Kartono, A. *et al.* (2007) Mutations in the gene encoding the basal body protein RPGRIP1L, a nephrocystin-4 interactor, cause Joubert syndrome. *Nat. Genet.*, **39**, 882–888.
15. Delous, M., Baala, L., Salomon, R., Laclef, C., Vierkotten, J., Tory, K., Golzio, C., Lacoste, T., Besse, L., Ozilou, C. *et al.* (2007) The ciliary gene *RPGRIP1L* is mutated in cerebello-oculo-renal syndrome (Joubert syndrome type B) and Meckel syndrome. *Nat. Genet.*, **39**, 875–881.
16. Brancati, F., Travaglini, L., Zablocka, D., Boltshauser, E., Accorsi, P., Montagna, G., Silhavy, J.L., Barrano, G., Bertini, E., Emma, F. *et al.* (2008) RPGRIP1L mutations are mainly associated with the cerebello-renal phenotype of Joubert syndrome-related disorders. *Clin. Genet.*, **74**, 164–170.
17. Doherty, D., Parisi, M.A., Finn, L.S., Gunay-Aygun, M., Al-Mateen, M., Bates, D., Clericuzio, C., Demir, H., Dorschner, M., van Essen, A.J. *et al.* (2009) Mutations in 3 genes (MKS3, CC2D2A and RPGRIP1L) cause COACH syndrome (Joubert syndrome with congenital hepatic fibrosis). *J. Med. Genet.*, **47**, 8–21.
18. Tallila, J., Jakkula, E., Peltonen, L., Salonen, R. and Kestila, M. (2008) Identification of CC2D2A as a Meckel syndrome gene adds an important piece to the ciliopathy puzzle. *Am. J. Hum. Genet.*, **82**, 1361–1367.
19. Noor, A., Windpassinger, C., Patel, M., Stachowiak, B., Mikhailov, A., Azam, M., Irfan, M., Siddiqui, Z.K., Naeem, F., Paterson, A.D. *et al.* (2008) CC2D2A, encoding a coiled-coil and C2 domain protein, causes autosomal-recessive mental retardation with retinitis pigmentosa. *Am. J. Hum. Genet.*, **82**, 1011–1018.
20. Gorden, N.T., Arts, H.H., Parisi, M.A., Coene, K.L., Letteboer, S.J., van Beersum, S.E., Mans, D.A., Hikida, A., Eckert, M., Knutzen, D. *et al.* (2008) *CC2D2A* is mutated in Joubert Syndrome and interacts with the ciliopathy-associated basal body protein CEP290. *Am. J. Hum. Genet.*, **83**, 559–571.
21. Noor, A., Windpassinger, C., Patel, M., Stachowiak, B., Mikhailov, A., Azam, M., Irfan, M., Paterson, A.D., Lutufullah, M., Doherty, D. *et al.* (2008) Addendum. CC2D2A, encoding a coiled-coil and C2 domain protein, causes autosomal-recessive mental retardation with retinitis pigmentosa. *Am. J. Hum. Genet.*, **83**, 656.
22. Tallila, J., Salonen, R., Kohlschmidt, N., Peltonen, L. and Kestila, M. (2009) Mutation spectrum of Meckel syndrome genes: one group of syndromes or several distinct groups?. *Hum. Mutat.*, **30**, E813–E830.
23. Valente, E.M., Logan, C.V., Mougou-Zerelli, S., Lee, J.H., Silhavy, J.L., Brancati, F., Iannicelli, M., Travaglini, L., Romani, S., Illi, B. *et al.* (2010) Mutations in *TMEM216* perturb ciliogenesis and cause Joubert, Meckel and related syndromes. *Nat. Genet.*, **42**, 619–625.
24. Edvardson, S., Shaag, A., Zenvirt, S., Erlich, Y., Hannon, G.J., Shanske, A.L., Gomori, J.M., Ekstein, J. and Elpeleg, O. (2010) Joubert syndrome 2 (JBTS2) in Ashkenazi Jews is associated with a TMEM216 mutation. *Am. J. Hum. Genet.*, **86**, 93–97.
25. Bergmann, C., Fliegauf, M., Bruchle, N.O., Frank, V., Olbrich, H., Kirschner, J., Schermer, B., Schmedding, I., Kispert, A., Kranzlin, B. *et al.* (2008) Loss of nephrocystin-3 function can cause embryonic lethality, Meckel-Gruber-like syndrome, situs inversus, and renal-hepatic-pancreatic dysplasia. *Am. J. Hum. Genet.*, **82**, 959–970.
26. Karmous-Benailly, H., Martinovic, J., Gubler, M.C., Sirot, Y., Clech, L., Ozilou, C., Auge, J., Brahimi, N., Etchevers, H., Detrait, E. *et al.* (2005) Antenatal presentation of Bardet-Biedl syndrome may mimic Meckel syndrome. *Am. J. Hum. Genet.*, **76**, 493–504.
27. Hildebrandt, F., Attanasio, M. and Otto, E. (2009) Nephronophthisis: disease mechanisms of a ciliopathy. *J. Am. Soc. Nephrol.*, **20**, 23–35.
28. Vierkotten, J., Dildrop, R., Peters, T., Wang, B. and Ruther, U. (2007) Ftm is a novel basal body protein of cilia involved in Shh signalling. *Development*, **134**, 2569–2577.
29. Dawe, H.R., Smith, U.M., Cullinane, A.R., Gerrelli, D., Cox, P., Badano, J.L., Blair-Reid, S., Sriram, N., Katsanis, N., Attie-Bitach, T. *et al.* (2007) The Meckel-Gruber Syndrome proteins MKS1 and meckelin interact and are required for primary cilium formation. *Hum. Mol. Genet.*, **16**, 173–186.
30. Bialas, N.J., Inglis, P.N., Li, C., Robinson, J.F., Parker, J.D., Healey, M.P., Davis, E.E., Inglis, C.D., Toivonen, T., Cottell, D.C. *et al.* (2009) Functional interactions between the ciliopathy-associated Meckel syndrome 1 (MKS1) protein and two novel MKS1-related (MKSR) proteins. *J. Cell Sci.*, **122**, 611–624.
31. Tammachote, R., Hommerding, C.J., Sinders, R.M., Miller, C.A., Czarnecki, P.G., Leightner, A.L., Salisbury, J.L., Ward, C.J., Torres, V.E., Gattone, V.H. 2nd *et al.* (2009) Ciliary and centrosomal defects associated with mutation and depletion of the Meckel syndrome genes *MKS1* and *MKS3*. *Hum. Mol. Genet.*, **18**, 3311–3323.
32. Tsang, W.Y., Bossard, C., Khanna, H., Peranen, J., Swaroop, A., Malhotra, V. and Dynlacht, B.D. (2008) CP110 suppresses primary cilia formation through its interaction with CEP290, a protein deficient in human ciliary disease. *Dev. Cell*, **15**, 187–197.
33. Weatherbee, S.D., Niswander, L.A. and Anderson, K.V. (2009) A mouse model for Meckel Syndrome reveals Mks1 is required for ciliogenesis and Hedgehog signaling. *Hum. Mol. Genet.*, **18**, 4565–4575.
34. Williams, C.L., Winkelbauer, M.E., Schafer, J.C., Michaud, E.J. and Yoder, B.K. (2008) Functional redundancy of the B9 proteins and nephrocystins in C. elegans ciliogenesis. *Mol. Biol. Cell*, **19**, 2154–2168.
35. Ng, S.B., Buckingham, K.J., Lee, C., Bigham, A.W., Tabor, H.K., Dent, K.M., Huff, C.D., Shannon, P.T., Jabs, E.W., Nickerson, D.A. *et al.* (2010) Exome sequencing identifies the cause of a mendelian disorder. *Nat. Genet.*, **42**, 30–35.
36. Sanders, S. (2011) Whole-exome sequencing: a powerful technique for identifying novel genes of complex disorders. *Clin. Genet.*, **79**, 132–133.
37. Walsh, T., Lee, M.K., Casadei, S., Thornton, A.M., Stray, S.M., Pennil, C., Nord, A.S., Mandell, J.B., Swisher, E.M. and King, M.C. (2010) Detection of inherited mutations for breast and ovarian cancer using genomic capture and massively parallel sequencing. *Proc. Natl Acad. Sci. USA*, **107**, 12629–12633.
38. Consugar, M.B., Kubly, V.J., Lager, D.J., Hommerding, C.J., Wong, W.C., Bakker, E., Gattone, V.H. 2nd, Torres, V.E., Breuning, M.H. and

Harris, P.C. (2007) Molecular diagnostics of Meckel-Gruber syndrome highlights phenotypic differences between MKS1 and MKS3. *Hum. Genet.*, **121**, 591–599.
39. Brouzes, E., Medkova, M., Savenelli, N., Marran, D., Twardowski, M., Hutchison, J.B., Rothberg, J.M., Link, D.R., Perrimon, N. and Samuels, M.L. (2009) Droplet microfluidic technology for single-cell high-throughput screening. *Proc. Natl Acad. Sci. USA*, **106**, 14195–14200.
40. Tewhey, R., Warner, J.B., Nakano, M., Libby, B., Medkova, M., David, P.H., Kotsopoulos, S.K., Samuels, M.L., Hutchison, J.B., Larson, J.W. *et al.* (2009) Microdroplet-based PCR enrichment for large-scale targeted sequencing. *Nat. Biotechnol.*, **27**, 1025–1031.
41. Kim, J., Krishnaswami, S.R. and Gleeson, J.G. (2008) CEP290 interacts with the centriolar satellite component PCM-1 and is required for Rab8 localization to the primary cilium. *Hum. Mol. Genet.*, **17**, 3796–3805.
42. Li, S., Armstrong, C.M., Bertin, N., Ge, H., Milstein, S., Boxem, M., Vidalain, P.O., Han, J.D., Chesneau, A., Hao, T. *et al.* (2004) A map of the interactome network of the metazoan C. elegans. *Science*, **303**, 540–543.
43. Ponsard, C., Skowron-Zwarg, M., Seltzer, V., Perret, E., Gallinger, J., Fisch, C., Dupuis-Williams, P., Caruso, N., Middendorp, S. and Tournier, F. (2007) Identification of ICIS-1, a new protein involved in cilia stability. *Front Biosci.*, **12**, 1661–1669.
44. Town, T., Breunig, J.J., Sarkisian, M.R., Spilianakis, C., Ayoub, A.E., Liu, X., Ferrandino, A.F., Gallagher, A.R., Li, M.O., Rakic, P. *et al.* (2008) The *stumpy* gene is required for mammalian ciliogenesis. *Proc. Natl Acad. Sci. USA*, **105**, 2853–2858.
45. Moyer, J.H., Lee-Tischler, M.J., Kwon, H.-Y., Schrick, J.J., Avner, E.D., Sweeney, W.E., Godfrey, V.L., Cacheiro, N.L.A., Wilkinson, J.E. and Woychik, R.P. (1994) Candidate gene associated with a mutation causing recessive polycystic kidney disease in mice. *Science*, **263**, 1329–1333.
46. Cui, C., Chatterjee, B., Francis, D., Yu, Q., Sanagustin, J.T., Francis, R., Tansey, T., Charisse, H., Wang, B., Lemley, B. *et al.* (2010) Disruption of Mks1 localization to the mother centriole causes cilia defects and developmental malformations in Meckel-Gruber syndrome. *Dis. Model Mech.*, **4**, 43–56.
47. Katsanis, N., Ansley, S.J., Badano, J.L., Eichers, E.R., Lewis, R.A., Hoskins, B.E., Scambler, P.J., Davidson, W.S., Beales, P.L. and Lupski, J.R. (2001) Triallelic inheritance in Bardet-Biedl syndrome, a Mendelian recessive disorder. *Science*, **293**, 2256–2259.
48. Leitch, C.C., Zaghloul, N.A., Davis, E.E., Stoetzel, C., Diaz-Font, A., Rix, S., Al-Fadhel, M., Lewis, R.A., Eyaid, W., Banin, E. *et al.* (2008) Hypomorphic mutations in syndromic encephalocele genes are associated with Bardet-Biedl syndrome. *Nat. Genet.*, **40**, 443–448.
49. Davis, E.E., Zhang, Q., Liu, Q., Diplas, B.H., Davey, L.M., Hartley, J., Stoetzel, C., Szymanska, K., Ramaswami, G., Logan, C.V. *et al.* (2011) TTC21B contributes both causal and modifying alleles across the ciliopathy spectrum. *Nat. Genet.*, **43**, 189–196.
50. Kim, J., Lee, J.E., Heynen-Genel, S., Suyama, E., Ono, K., Lee, K., Ideker, T., Aza-Blanc, P. and Gleeson, J.G. (2010) Functional genomic screen for modulators of ciliogenesis and cilium length. *Nature*, **464**, 1048–1051.
51. Rossetti, S., Torra, R., Coto, E., Consugar, M., Kubly, V., Malaga, S., Narvarro, M., El-Youssef, M., Torres, V. and Harris, P.C. (2003) A complete mutation screen of *PKHD1* in autosomal recessive polycystic kidney pedigrees. *Kidney Int.*, **64**, 391–403.
52. Otto, E.A., Ramaswami, G., Janssen, S., Chaki, M., Allen, S.J., Zhou, W., Airik, R., Hurd, T.W., Ghosh, A.K., Wolf, M.T. *et al.* (2011) Mutation analysis of 18 nephronophthisis associated ciliopathy disease genes using a DNA pooling and next generation sequencing strategy. *J. Med. Genet.*, **48**, 105–116.
53. Inglis, P.N., Boroevich, K.A. and Leroux, M.R. (2006) Piecing together a ciliome. *Trends Genet.*, **22**, 491–500.
54. Rossetti, S., Kubly, V.J., Consugar, M.B., Hopp, K., Roy, S., Horsley, S.W., Chauveau, D., Rees, L., Barratt, T.M., van't Hoff, W.G. *et al.* (2009) Incompletely penetrant PKD1 alleles suggest a role for gene dosage in cyst initiation in polycystic kidney disease. *Kidney Int.*, **75**, 848–855.